Native defects in second-generation topological insulators: Effect of spin-orbit interaction on Bi_{2}Se_{3}

D. West, Y. Y. Sun, Han Wang, Junhyeok Bang, and S. B. Zhang

Native Defects in Second Generation Topological Insulators: The Effect of Spin-Orbit Interaction on Bi$_2$Se$_3$

D. West, Y. Y. Sun, Han Wang, Junhyeok Bang, and S. B. Zhang

Department of Physics, Applied Physics, and Astronomy, Rensselaer Polytechnic Institute, Troy, New York 12180, USA

Abstract

Native defects in pnictogen chalcogenides are currently a great barrier toward the realization of the exotic properties of this class of topological insulators. Previous first-principles results of low-energy defects in Bi$_2$Te$_3$ and Sb$_2$Te$_3$ are in qualitative agreement with experiments. However, for Bi$_2$Se$_3$ the calculated low-energy defects are antisites, opposed to Se vacancy (V$_{Se}$) as observed experimentally. We find that the inclusion of spin-orbit interaction drastically shift the band-edge energies of the bulk states with respect to defect transition energies. It turns Bi antisite (Bi$_{Se}$) from an acceptor to a donor and makes V$_{Se}$ more stable than Bi$_{Se}$. This brings the calculated results for native defects in pnictogen chalcogenides into agreement with experiments.

Topological insulators (TI) have recently emerged as a new class of materials[1,2,3,4,5,6] with energy gaps in the bulk but metallic states on the surface. The linear dispersion of the surface states near the Fermi energy gives rise to Dirac fermion behavior, which can be beneficial for the transport of the charge carriers. The Dirac fermions are protected by time-reversal symmetry, therefore are robust against defect formation, disorder, surface contamination, and any change in the operation conditions – provided such perturbations are not large enough to alter the topological nature of the material. The realization of three-dimensional TIs has triggered a series of research that touches the most profound aspects of modern physics, such as non-Maxwell electrodynamics, magnetic monopoles, and Majorana fermions.[7,8,9,10,11,12,13] It has also been suggested that the chiral topological surface states[14] are protected from backscattering and localization in the presence of non-magnetic disorders and impurities with potential applications in spintronics and quantum computing[15,16].

However, despite the resolution of such surface states via angle resolved photoemission spectroscopy (ARPES) measurements – many of the predicted exotic properties are still elusive. One of the primary difficulties is in the control of the Fermi energy. Although the surface states are robust against disorder and perturbations which do not destroy the bulk band structure, this only true if the bulk is gapped. The small band-gap of the 3D topological insulators (on the order of SO interaction) makes it easy to form native defects inside the bulk material. Experimentally, this leads to the situation wherein the Fermi energy is often in the bulk conduction or valence bands. It is of great current interest and technological importance to control native defects in these materials in order to bring the bulk Fermi energy in line with the Dirac point on the surface.

In this paper, first-principles calculations are applied to study the formation energy (ΔH) of native defects in Bi_2Se_3, Bi_2Te_3, and Sb_2Te_3. We show that the defect responsible for the native conductivity in each instance changes with growth condition. Under the cation-rich growth conditions, V_{Se}, Bi_{Te}, and Sb_{Te} are responsible for the native (n-, p-, and n-) type conductivity of Bi_2Se_3, Bi_2Te_3, and Sb_2Te_3, respectively. Under the anion-rich conditions, on the other hand, Se_{Bi}, Te_{Bi}, and V_{Sb} are responsible for the native (n-, n-, and p-) type conductivity. Our results correctly predict the observed n-type, n-p transition, and p-type conductivity in Bi_2Se_3, Bi_2Te_3, and Sb_2Te_3, respectively. In contrast to ordinary semiconductors, however, the inclusion of the spin-orbit interaction (SOI) is not only necessary to describe the topological nature for these materials, but it becomes equally important in the determination of the defect properties; in particular, the inclusion of the SOI qualitatively alters the prediction for Bi_2Se_3 from native p-type to native n-type.

Our calculations are based on the density functional theory within the Perdew-Burke-Ernzerhof approximation.[17] Interactions between ion cores and valence electrons are described by the projector augmented wave (PAW) method,[18,19] as implemented in the VASP package.[20,21] Plane-waves with a kinetic energy cutoff of 250 eV were used as the basis set. The SOI was implemented in the all-electron part of the PAW Hamiltonian within the muffin tin spheres. We used a (4x4) unit cell with three quintuple slabs containing 95 Bi (or Sb) and 145 Te (or Se) atoms, and one special k-point at (7/24, 1/12, 0). It yields a total-energy convergence better than 0.02 eV per supercell, as compared with calculations using a (3x3x1) Monkhorst-Pack k-point grid.[22] The convergence criterion for the atomic structural relaxations within the fixed cells is 0.025 eV/Å.

The defect formation energy is calculated according to,[23]

$$\Delta H = E(D^q) - E_{bulk} + \sum_i \Delta n_i \mu_i + q(E_F + E_{VBM}), \qquad (1)$$

where $E(D^q)$ represents the energy of the supercell containing the defect in charge state, q, E_{bulk} is the energy of the defect-free bulk supercell, and μ_i is the chemical potential of the ith atomic species of which the number of have changed by Δn_i in the formation of the defect. Under the cation (anion) rich growth conditions, the chemical potential of the cation (anion) is determined from its bulk phase, while the chemical potential of the anion (cation) is determined such that $2\mu_C + 3\mu_A = \mu_{2C3A}$, where μ_{2C3A} is the chemical potential of the binary. In our calculations, the hexagonal scalenohedral phases of Bi and Sb, as well as the trigonal-trapezohedral phases of Te and Se, from ref [24], were used as the reference elemental bulk phases for the chemical potentials.

All the three materials, Bi_2Se_3, Bi_2Te_3, and Sb_2Te_3 have the same R-3m space-group symmetry and consist of a layered structure of quintuple layers (QL)[4], as seen in Fig. 1. Each QL terminates with Te or Se: for example in a sequence SeI-Bi-SeII-Bi-SeI for Bi_2Se_3. The band structure of each material is shown in Fig. 2: the bands without SOI are indicated by dashed lines, while those with SOI are indicated by solid lines. The energy zero corresponds to the Fermi energy of the SOI calculation. The alignment between the SOI and non-SOI band structures shown assumes that the change in charge density due to the SOI interaction is small enough that it does not change the average electrostatic potential of the cell. Without SOI, each material is an ordinary insulator with a direct band gap. The calculated partial density of states reveals that the CBM is predominately cation (Bi or Sb) and the VBM is predominately anion (Te or Se) in character. After inclusion of the SOI, the gap opens up. The characters of the VBM and CBM states invert at the Γ point, reflecting the topological nature of these materials.

Importantly, in all three cases, the VBM and CBM are substantially lowered relative to the non spin-orbit case, with the new CBM nearly coincides with the VBM of the non spin-orbit case.

The formation energies of the low-energy vacancies and antisites as a function of Fermi energy are shown in Fig. 3(a)-(c) under the cation-rich growth conditions (top) and under the anion-rich growth conditions (bottom). The pink (lightly shaded) region corresponds to the SOI results; the gray (darkly shaded) region corresponds to the non-SOI results. The alignment between the SOI and non SOI energies is obtained from the band structure calculations in Fig. 2. Note that there is no overlap in the band gaps between SOI and non SOI results. Besides the defects in the figure, we also calculated interstitial defects. However, they were found to be high in energy in excess of at least 2 eV and can hence be ignored. For defects on the anion sites: V_{Te}, V_{Se}, Sb_{Te}, Bi_{Te}, and Bi_{Se}, there are two inequivalent lattice sites, I and II (see Fig. 1). In all cases, the low-energy defects were found to correspond to site I (namely, replacing or removing the anion at the surface of a QL). This can be expected as an anion at the center of a QL with 6 bonds should be more stable than the one on the surface with three bonds. The extent to which the surface defect was more stable was found to depend on defect and material, ranging from .2~.3 eV in Sb_2Te_3 to .4~.9 eV in Bi_2Se_3.

It appears that SOI has significant effects on the defect behavior, particularly for Bi_2Se_3. Without the SOI, the two competing low-energy defects under the Bi-rich growth conditions are the relatively-deep donor, V_{Se}^{2+}, and shallow acceptor, Bi_{Se}^-. The fact that they cross near the VBM implies that Bi_2Se_3 should have native p-type conductance which is at odds with available experiments, which consistently show that stoichiometric Bi_2Se_3 is n-type. However, within the SOI calculation, this result is reversed. Not only does V_{Se} become shallow and the dominate low-energy defect (consistent with transport and STM measurements which have suggested the

presence of Se vacancies [25, 26]) but Bi_{Se} also changes type from being an acceptor to being a donor.

One may argue that atomic relaxation or some other unknown mechanism, such as a significantly altered bonding strength due to SOI, plays the key role in changing the defect behaviors. However, judging from Fig. 3, these are unlikely because the changes in the defect energy are typically less than 0.1 eV. (The extent to which such effects are important will be discussed below with Fig. 4.) Rather, the qualitative changes, including the conversion of the defect type from acceptors to donors, can be understood almost exclusively by the shift of the VBM (and CBM) in the presence of the SOI, despite that the shift is only modest, 0.3 eV in the case of Bi_2Se_3. The reason is because a downward shift in the VBM lowers the energies of the donors and simultaneously increases the energy of the acceptors. This effect may be seen most clearly for Sb_2Te_3 in Fig. 3(c) where the results of SOI connect nearly perfectly with those of non-SOI in the small-gaped region on the horizontal axis. The increased donor stability due to VBM lowering is also seen in Bi_2Te_3 where V_{Te} emerges as a donor in the SOI calculation oppose to being charge neutral in the non-SOI calculation.

From either SOI or non SOI calculation, it can be seen that native defects in pnictogen chalcogenides have relatively low ΔH. Hence, higher native defect and associated carrier concentrations than those in ordinary semiconductors may be expected. Our analysis below for *neutral* charge defects reveals that the relatively low defect energy stems from the rather low bulk formation energies, whose already small values of -1.13, -1.90, and -0.6 eV per formula unit (C_2A_3) for Bi_2Te_3, Bi_2Se_3, and Sb_2Te_3 are reduced to -0.84, -1.52, and -0.56 eV, respectively, due to SOI. We consider neutral defects because the aforementioned effect due to VBM shift vanishes [cf. Eq. (1)].

6

Figure 4 shows ΔH for defects, in which circles correspond to results without SOI and squares correspond to results with SOI. The materials are arranged from left to right along the horizontal axis with increasing bulk formation energy (and cohesive energy): $Sb_2Te_3 \rightarrow Bi_2Te_3 \rightarrow Bi_2Se_3$. As ΔH for bulk increases, one might expect ΔH for the associated defects to increase as well. Indeed, this is the general trend observed in Fig. 4. Moreover, the effect for cation-site defects (V_C and A_C) under the cation-rich growth conditions is significantly larger than that under the anion-rich growth conditions. Conversely, the effect for anion-site defect (C_A) under the anion-rich growth conditions is significantly larger than that under the cation-rich growth conditions. V_A is somewhat an exception: under the anion-rich growth conditions, $\Delta H(V_A)$ also increases with bulk ΔH; however, because the increase is so small, $\Delta H(V_A)$ decreases under the cation-rich growth conditions. The V_A is characterized by cation lone pairs. This "abnormal" result suggests that Bi lone pair may be more stable than Sb lone pair.

From the calculated ΔH we can estimate the concentrations for native defects. Assuming a growth temperature of 600K, Table 1 lists the calculated type of native conductivity as well as the estimated concentration of the dominate defect. Although generally native defect concentrations are high, the two most promising combinations of materials and growth conditions, namely, Sb_2Te_3 grown under the Te rich conditions and Bi_2Se_3 grown under the Se-rich conditions have calculated defect concentrations of only 10^{18} and 10^{17} cm^{-3}. This suggests that we still have considerable room to improve the qualities of the pnictogen chalcogenides by carefully approaching equilibrium growth conditions.

In summary, by first-principles calculations, we identify the defects responsible for the experimentally observed native (n-, n-p transition, p-) type conductivity of Bi_2Se_3, Bi_2Te_3, and Sb_2Te_3. Under the cation-rich growth conditions, the dominate defects in these materials are

V_{Se}^{2+}, Bi_{Te}^{-}, and Sb_{Te}^{-}, respectively, while under the anion-rich growth conditions, they are Se_{Bi}^{+}, Te_{Bi}^{+}, and V_{Sb}^{-}. For Bi_2Te_3 and Sb_2Te_3 these conclusions agree with previous non-SOI work. However, the inclusion of SOI is vital to the explanation of native n-type conductivity in Bi_2Se_3. We identify the primary role of the SOI on the formation of native defects as the displacement of the band-edge energies with respect to those without the SOI.
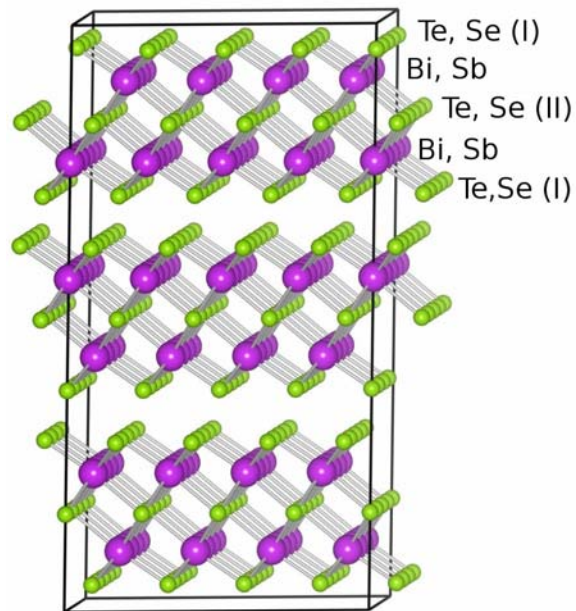
Figure 1: A 240-atom supercell containing three 4x4 quintuple layers used for defect calculations. The cation, either Bi or Sb, is represented by the large spheres, and the anion, either Te or Se, is represented by the small spheres. There are two inequivalent Te (Se) positions, labeled I (e.g., on the surface of a QL) and II (e.g., at the center of a QL).
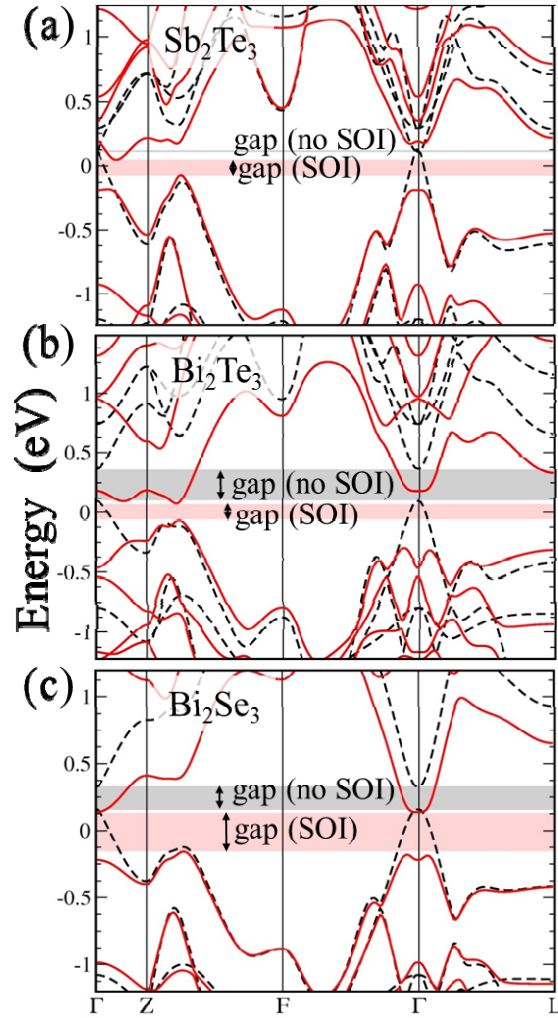
Figure 2: (color online) Bulk band structure of (a) Sb_2Te_3, (b) Bi_2Te_3, and (c) Bi_2Se_3 calculated without SOI (dashed curves) and with SOI (solid curves). The band gap with and without SOI is indicated by the pink (light shaded) and gray (dark shaded) regions, respectively.
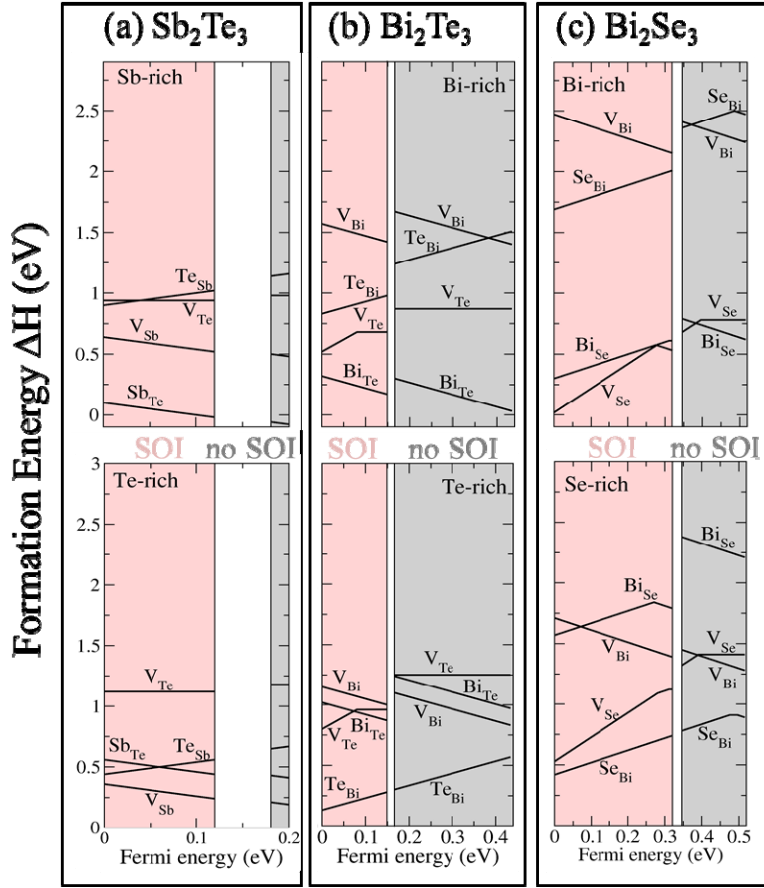
Figure 3: Formation energy of native defects in (a) Sb_2Te_3, (b) Bi_2Te_3, and (c) Bi_2Se_3, respectively, under (upper) cation-rich and (lower) anion-rich growth conditions. The shaded and unshaded regions indicate the formation energies calculated with and without SOI. The offset between the two methods is inferred from the band-structure calculations shown in Fig 2.
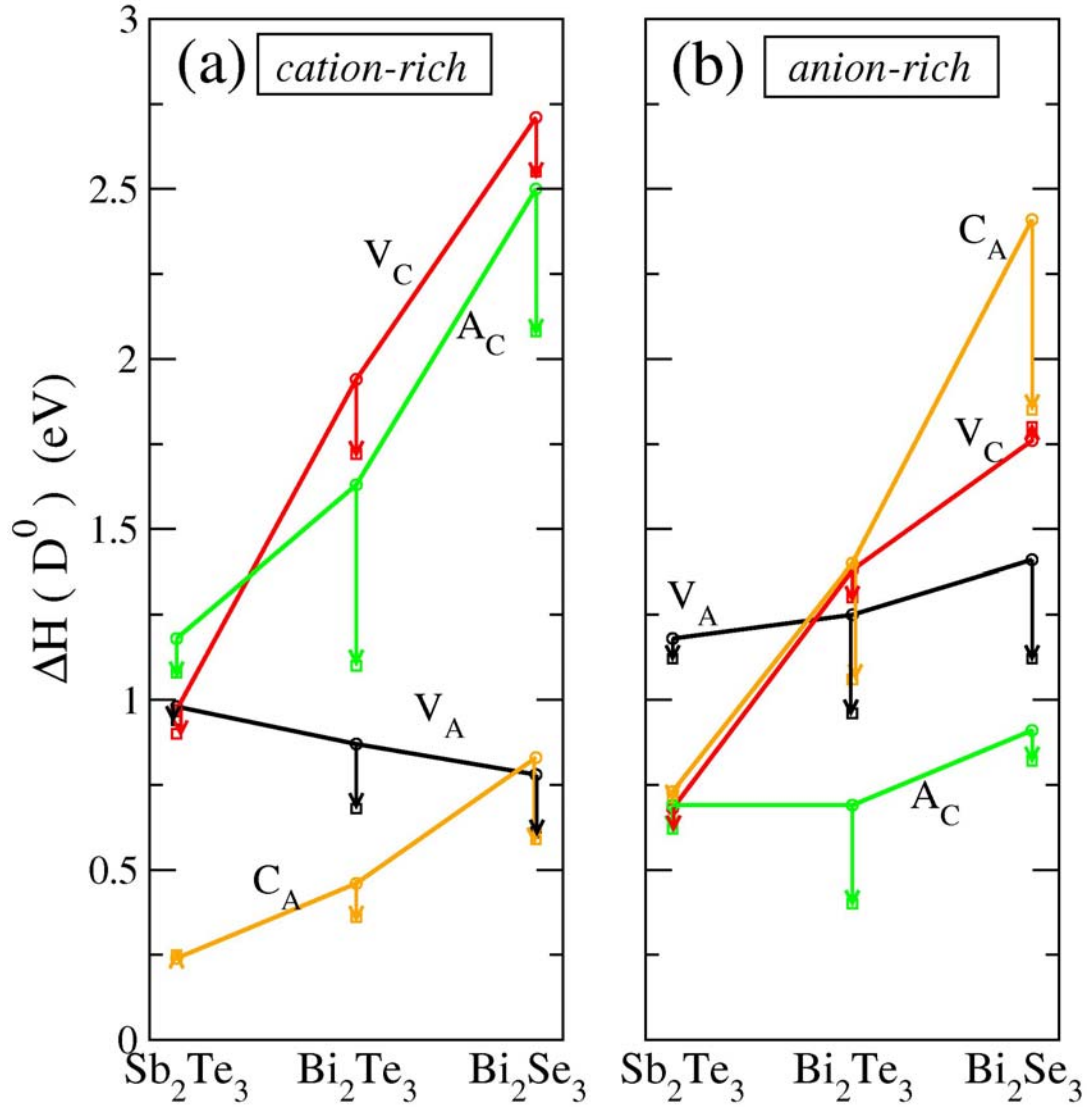
Figure 4: Formation energies of neutral defects without SOI (solid line and dot symbol) and those with SOI (square symbol) under (a) cation-rich and (b) anion-rich growth conditions. The change in ΔH is indicated by the vertical arrow. V_C, A_C, V_A, and C_A, represent cation vacancy, anion antisite, anion vacancy, and cation antisite, respectively. Along the horizontal axis from Sb_2Te_3 to Bi_2Se_3, the formation energy, as well as the cohesive energy, of the bulk material increases.

Table 1: Calculated conductivity type and estimated concentration in cm^{-3} of the dominate defect. In the estimation, Fermi level has been assumed to be at the midgap during growth at 600K.

	cation-rich	anion-rich
Bi_2Te_3	(p) 8×10^{19}	(n) 2×10^{20}
Bi_2Se_3	(n) 3×10^{19}	(n) 2×10^{17}
Sb_2Te_3	(p) 2×10^{21}	(p) 2×10^{18}

[1] B. A. Bernevig, T. L. Hughes, and S.-C. Zhang, Science **314**, 1757 (2006).

[2] L. Fu and C. L. Kane, Phys. Rev. B **76**, 045302 (2007).

[3] Y. L. Chen, J. G. Analytis, J.-H. Chu, Z. K. Liu, S.-K. Mo, X. L. Qi, H. J. Zhang, D. H. Lu, X. Dai, Z. Fang, S. C. Zhang, I. R. Fisher, Z. Hussain, and Z.-X. Shen, Science **325**, 178 (2009).

[4] H. Zhang, C.-X. Liu, X.-L. Qi, X. Dai, Z. Fang, and S.-C. Zhang, Nat. Phys. **5**, 438 (2009).

[5] Y. Xia, D. Qian, D. Hsieh, L. Wray, A. Pal, H. Lin, A. Bansil, D. Grauer, Y. S. Hor, R. J. Cava, and M. Z. Hasan, Nat. Phys. **5**, 398 (2009).

[6] X.-L. Qi, T. L. Hughes, and S.-C. Zhang, Phys. Rev. B **78**, 195424 (2008).

[7] X.-L. Qi and S.-C. Zhang, Phys. Today, p33-p38 (Jan. 2010),

[8] M. Z. Hasan and C. L. Kane, **arXiv**:1002.3895 (2010).

[9] J. E. Moore, Nature **464**, 194 (2010).

[10] X.-L. Qi, R. Li, J. Zhang, and S.-C. Zhang, Science **323**, 1184 (2009).

[11] L. Fu and C. L. Kane, Phys. Rev. Lett. **100**, 096407 (2008).

[12] A. R. Akhmerov, J. Nilsson, and C. W. J. Beenakker, Phys. Rev Lett. **102**, 216404 (2009).

[13] L. Fu and C. L. Kane, Phys. Rev. Lett. **102**, 216403 (2009).

[14] D. Hsieh, Y. Xia, L.Wray, D. Qian, A. Pal, J. H. Dil, J. Osterwalder, F. Meier, G. Bihlmayer, C. L. Kane, Y. S. Hor, R. J. Cava, and M. Z. Hasan, Science **323**, 919 (2009).

[15] P. Roushan, J. Seo, C. V. Parker, Y. S. Hor, D. Hsieh, D. Qian, A. Richardella, M. Z. Hasan, R. J. Cava, and A. Yazdani, Nature **460**, 1106 (2009).

[16] T. Zhang, P. Cheng, Xi Chen, J.-F. Jia, X. Ma, Ke He, L. Wang, H. Zhang, Xi Dai, Z. Fang, X. Xie, and Q.-K. Xue, Phys. Rev. Lett. **103**, 266803 (2009).

[17] J. P. Perdew, K. Burke, and M. Ernzerhof, Phys. Rev. Lett. 77, 3865 (1996).

[18] P. E. Blochl, Phys. Rev. B **50**, 17953 (1994).

[19] G. Kresse and D. Joubert, Phys. Rev. B **59**, 1758 (1999).

[20] G. Kresse and J. Hafner, Phys. Rev. B **47**, 558 (1993).

[21] G. Kresse and J. Furthmuller, Phys. Rev. B **54**, 11169 (1996).

[22] H. J. Monkhorst and J. D. Pack, Phys. Rev. B **13**, 5188 (1976).

[23] S. B. Zhang and J. E. Northrup, Phys. Rev. Lett. **67**, 2339 (1991).

[24] R. W. G. Wyckoff, *Crystal Structures* (Interscience Publishers, New York, 1963), second edition Vol. 1, p. 7-83.

[25] J. Navratil, J. Horak, T. Plechacek, S. Kamba, P. Lostak, J.S. Dyck, W. Chen, and C. Uher, J. of Solid State Chem. 177, 1704 (2004).

[26] Z. Alpichshev, R. Biswas, A. V. Balatsky, J. G. analytis, J.-H Chu, I.R. Fisher, A. Kapitulnik, Phys. Rev. Lett. 108, 206402 (2012).